Partially Absorbed Comptonization Spectrum from the Nearly Edge-on Source X1822-371

Iaria, R.; di Salvo, T.; Burderi, L.; Robba, N.R.

Published in:
Astrophysical Journal

DOI:
10.1086/321645

THE ASTROPHYSICAL JOURNAL, 557:24–29, 2001 August 10

PARTIALLY ABSORBED COMPTONIZATION SPECTRUM FROM THE NEARLY EDGE-ON SOURCE X1822−371

R. IARIA,[1] T. DI SALVO,[1,2] L. BURDERI,[3] AND N. R. ROBBA[1]

Received 2001 February 23; accepted 2001 April 12

ABSTRACT

We report the results of a spectral analysis over the range 0.1–200 keV performed on the dipping source X1822−371 observed by *BeppoSAX*. We find the best fit to the continuum using a partially covered Comptonization model, representing scattering of soft seed photons by electrons at a temperature of ∼4.8 keV, without the presence of any soft blackbody emission. The equivalent hydrogen column obtained for the absorbed component is $\sim 4.5 \times 10^{22}$ cm^{-2}, an order of magnitude larger than the Galactic absorption for this source, and the covering fraction is ∼71%. Because the inclination angle of X1822−371 to the line of sight is ∼85°, this model gives a reasonable scenario for the source: the Comptonized spectrum could come from an extended accretion disk corona (ADC), probably the only region that can be directly observed as a result of the high inclination. The excess matter producing the partial covering could be close to the equatorial plane of the system, above the outer disk, occulting the emission from the inner disk and the inner part of the ADC. An iron emission line is also present at ∼6.5 keV with an equivalent width of ∼150 eV. We argue that this strong iron line cannot be explained as reflection of the Comptonized spectrum by the accretion disk. It is probably produced in the ADC. An emission line at ∼1.9 keV (with an equivalent width of ∼54 eV) and an absorption edge at ∼8.7 keV (with an optical depth of ∼0.1) are also required to fit this spectrum. These features are probably produced by highly ionized iron (Fe XXIV) present in the outer part of the ADC, where the plasma density is $\sim 10^{11}$–10^{12} cm^{-3} and ionized plasma is present.

Subject headings: accretion, accretion disks — stars: individual (X1822−371) — stars: neutron — X-rays: general — X-rays: individual (1822−371) — X-rays: stars

1. INTRODUCTION

Low-mass X-ray binaries (LMXBs) consist of a low-mass star ($M \leq 1\ M_{\odot}$) and a neutron star, which generally has a weak magnetic field ($B \leq 10^{10}$ G). In these systems, the X-ray source is powered by accretion of mass overflowing the Roche lobe of the companion star and forming an accretion disk around the neutron star. Different inclinations of the line of sight with respect to the orbital plane can explain the different characteristics of the light curve observed in these systems. At low inclinations, eclipses and dips will not be visible in the light curves, while they can be present at high inclinations. About 10 LMXBs are known to show periodic dips in their X-ray light curves. The dip intensities, lengths, and shapes change from source to source and, for the same source, from cycle to cycle. Dips are probably due to a thicker region in the outer rim of the accretion disk, formed by the impact with the disk of the gas stream from the Roche lobe–filling companion star. For systems seen almost edge-on, X-ray emission is still visible because of the presence of an extended accretion disk corona (ADC; see White & Holt 1982), which can be periodically eclipsed by the companion star.

X1822−371 is an LMXB seen almost edge-on with an inclination angle of $i \sim 85°$ (Hellier & Mason 1989). Its light curve shows both dips and eclipses of the X-ray source by the companion star. The partial nature of the eclipse indicates that the X-ray–emitting region is extended and that the observed X-rays are scattered in an ADC. The 1–10 keV spectrum of X1822−371 as observed by *EXOSAT* was fitted by an absorbed blackbody plus a power-law component, with an iron emission line at ∼6.7 keV (Hellier & Mason 1989). The 1–30 keV spectrum observed by *Ginga* could not be described by the model above, which yielded a reduced χ^2 of 12 (Hellier, Mason, & Williams 1992), probably because of the better statistics and the wider energy range of *Ginga* with respect to *EXOSAT*. Other combinations of power-law, blackbody, and thermal bremsstrahlung were used to fit these data, but none of these models gave an acceptable fit. Heinz & Nowak (2001) analyzed simultaneous observations with *Rossi X-Ray Timing Explorer* (*RXTE*) and *ASCA* of X1822−371. They showed that both the source spectrum and light curve can be well fitted by two models, representing the case of an optically thick and optically thin corona, respectively. In the first case, no soft thermal component from the inner region contributes to the source spectrum, and the emission from the corona is described by a cutoff power law partially absorbed by a cold atmosphere above the disk. In the second case, the model consists of a blackbody component emitted from the central source and scattered into the line of sight by the optically thin corona and a cutoff power law emitted by the corona. Both these models could well describe the data, and therefore it was not possible to distinguish between them.

Recently, this source was studied by Parmar et al. (2000) using data from the *BeppoSAX* satellite in the energy range 0.3–40 keV. They fitted the spectrum using a Comptonization model with a seed photon temperature of ∼0.1 keV, an electron temperature of ∼4.5 keV, and a Comptonizing cloud optical depth of $\tau \sim 26$, as well as a strong

[1] Dipartimento di Scienze Fisiche ed Astronomiche, Università di Palermo, via Archirafi 36, I-90123 Palermo, Italy; iaria@gifco.fisica.unipa.it.

[2] Instituut "Anton Pannekoek," University of Amsterdam, and Center for High-Energy Astrophysics, Kruislaan 403, NL-1098 SJ Amsterdam, Netherlands.

[3] Osservatorio Astronomico di Roma, via Frascati 33, I-00040 Monteporzio Catone, Roma, Italy.

blackbody component at a temperature of ∼1.9 keV, which contributes more than 40% of the 0.3–40 keV flux of the source. An emission line at ∼6.5 keV and an absorption edge at ∼1.3 keV were also present. We have analyzed the same data using the whole *BeppoSAX* range (0.1–200 keV). We confirm that the model used by Parmar et al. (2000) can well fit the X1822−371 spectrum, but we find a better fit using a Comptonization model with partial covering, two emission lines at ∼6.5 and ∼1.9 keV, and an absorption edge at ∼8.7 keV. In our model there is no need for blackbody emission or an absorption edge at low energy.

2. OBSERVATIONS AND SPECTRAL ANALYSIS

The narrow-field instruments (NFIs) on board the *BeppoSAX* satellite (Boella et al. 1997) observed X1822−371 on 1997 September 9 and 10 for an effective exposure time of ∼43 ks. The NFIs are four co-aligned instruments that cover more than 3 decades of energy, from 0.1 up to 200 keV, with good spectral resolution in the whole range. The Low Energy Concentrator Spectrometer (LECS), operating in the range 0.1–10 keV, and the Medium Energy Concentrator Spectrometer (MECS; 1–11 keV) have imaging capabilities with fields of view of radius 20′ and 30′, respectively. We selected data for analysis in circular regions centered on the source of 8′ and 4′ radii for the LECS and MECS, respectively. The background subtraction was obtained using blank-sky observations in which we extracted the background spectra in regions of the field of view similar to those used for the source. The High Pressure Gas Scintillation Proportional Counter (HPGSPC; 7–60 keV) and the Phoswich Detection System (PDS; 13–200 keV) are nonimaging instruments, because their fields of view (∼1° FWHM) are delimited by collimators. In the spectral analysis we used the standard energy ranges for the NFIs, which are 0.12–4 keV for the LECS, 1.8–10 keV for the MECS, 7–30 keV for the HPGSPC, and 15–200 keV for the PDS. As is customary, in the spectral fitting procedure we allowed for different normalizations in the LECS, HPGSPC, and PDS spectra relative to the MECS spectrum and checked a posteriori that derived values are in the standard range for each instrument. We rebinned the energy spectra in order to have at least 30 counts per channel. The LECS and MECS spectra were further rebinned in order to oversample the full width at half-maximum of the energy resolution by a factor of 5 in the whole energy range.[4]

The observed average unabsorbed flux of the source in the 0.1–100 keV energy range is 1.55×10^{-9} ergs cm^{-2} s^{-1}. Adopting a distance of 2.5 kpc (Mason & Cordova 1982), this corresponds to an unabsorbed luminosity of 1.15×10^{36} ergs s^{-1}. This is compatible with the previously reported isotropic luminosity of the X-ray source of $\sim 10^{36}$ ergs s^{-1} (Mason & Cordova 1982).

In Figure 1 (*top*) we plot the X1822−371 light curve in the 1.8–10.5 keV energy band (MECS data) versus the orbital phase (using the orbital period reported by Parmar et al. 2000). In the light curve, a sinusoidal variation and a partial eclipse at an orbital phase of ∼0.8 are present. The hardness ratio (the ratio between the counts in the 4–8 and 1–4 keV energy bands; see Fig. 1, *bottom*) does not show large variations. Therefore, we performed our spectral

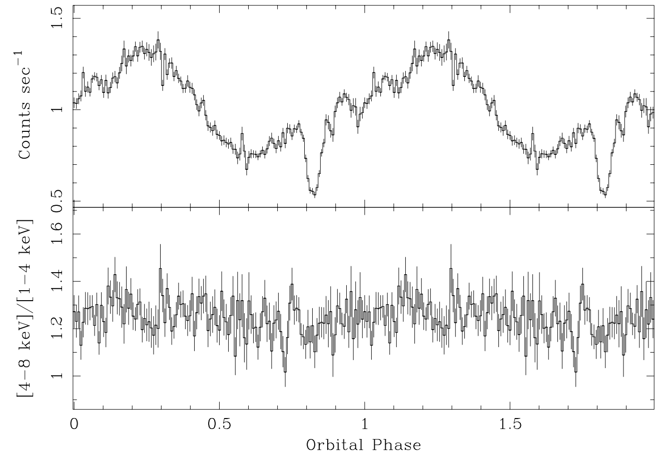

FIG. 1.—*Top*, folded light curve of X1822−371 in the 1.8–10 keV energy band (MECS data) vs. orbital phase; *Bottom*, ratio of the count rate in the 4–8 keV energy band with respect to that in 1–4 keV vs. orbital phase. Two cycles are shown for clarity.

analysis on the source spectrum averaged over all values of the orbital phase.

We fitted the model obtained by Parmar et al. (2000) in the energy range 0.3–40 keV to the *BeppoSAX* data in the energy range 0.12–200 keV. The model consists of photoelectric absorption by cold matter, a blackbody (BB), a Comptonized component ("Comptt"; Titarchuk 1994), an emission line at ∼6.5 keV, and an absorption edge at ∼1.3 keV. We obtained a $\chi^2/\text{dof} = 245/201$. The values of the parameters are compatible with the values obtained in the range 0.3–40 keV (Parmar et al. 2000) and are reported in Table 1 (see model 1). This model, however, presents two characteristics that are, in our opinion, hard to explain: the amount of photoelectric absorption, $N_{\rm H}$, and the luminosity of the blackbody component. The value of $N_{\rm H}$ reported by Parmar et al. (2000) is $\sim 1.2 \times 10^{20}$ cm^{-2}, an order of magnitude lower than the Galactic absorption expected in the direction of this source (see § 3). Using the whole *BeppoSAX* energy range, we find a larger value, $N_{\rm H} \sim 6 \times 10^{20}$ cm^{-2}, which is still smaller (by a factor of 1.7) than expected. Once again, a very low value of photoelectric absorption is found in the *RXTE* and *ASCA* data when the optically thin corona model (consisting of blackbody and cutoff power law) is used (Heinz & Nowak 2001). Moreover, the blackbody component in this model contributes more than 40% of the total source luminosity, which is quite large considering that the source is seen almost edge-on. Both these points have already been noted and discussed by Parmar et al. (2000).

We were therefore motivated to search for another model that could both best fit the data and have a simple physical interpretation. Thus, we repeated the analysis trying several models. In particular, given that the source is seen almost edge-on, we tried a Comptonization model ("Compst"; Sunyaev & Titarchuk 1980) with partial covering and an emission line at ∼6.5 keV. In this way, we obtained a $\chi^2/\text{dof} = 291/204$; the corresponding values of the parameters are reported in Table 1 (model 2). In Figure 2 (*top*) we present the *BeppoSAX* broadband spectrum and model 2, and in the same figure (*middle*) we show the residuals in units of σ with respect to model 2. In the residuals, an emission feature at ∼2 keV and an absorption feature at ∼10 keV are present. These residuals are of the order of

[4] See the *BeppoSAX* cookbook at http://www.asdc.asi.it/bepposax/software/index.html.

TABLE 1

Results of Fit of X1822−371 Spectrum in the 0.12–200 keV Energy Band

Parameter	Model 1 BB + Comptt + Line + Edge	Model 2 PC + Compst + Line	Model 3 PC + Compst + Line + Line + Edge	Model 4 PC + Comptt + Line + Line + Edge
$N_{\rm H}$ ($\times 10^{21}$ cm^{-2})	0.62 ± 0.20	1.43 ± 0.18	$1.23^{+0.16}_{-0.14}$	$1.09^{+0.26}_{-0.51}$
$N_{\rm H,PC}$ ($\times 10^{22}$ cm^{-2})	...	4.31 ± 0.27	4.45 ± 0.26	4.37 ± 0.31
f	...	0.688 ± 0.013	0.712 ± 0.016	$0.715^{+0.027}_{-0.022}$
$kT_{\rm BB}$ (keV)	1.590 ± 0.041	...	...	...
$N_{\rm BB}$	0.273 ± 0.014	...	...	...
kT_0 (keV)	$0.133^{+0.033}_{-0.038}$	...	...	<0.20
kT_e (keV)	$4.526^{+0.067}_{-0.065}$	$4.802^{+0.069}_{-0.067}$	4.724 ± 0.075	4.711 ± 0.075
τ	$24.22^{+0.87}_{-0.92}$	13.52 ± 0.26	13.81 ± 0.35	14.61 ± 0.37
$N_{\rm Comp}$ ($\times 10^{-2}$)	$2.09^{+0.21}_{-0.13}$	7.71 ± 0.30	7.67 ± 0.36	$6.22^{+3.88}_{-1.10}$
$f_{\rm bol}$	0.98×10^{-9}	1.53×10^{-9}	1.55×10^{-9}	1.49×10^{-9}
$E_{\rm Fe}$ (keV)	6.528 ± 0.046	6.523 ± 0.055	6.521 ± 0.050	6.520 ± 0.050
$\sigma_{\rm Fe}$ (keV)	$0.292^{+0.065}_{-0.062}$	$0.444^{+0.119}_{-0.086}$	$0.302^{+0.075}_{-0.068}$	$0.303^{+0.075}_{-0.068}$
$I_{\rm Fe}$ ($\times 10^{-3}$)	0.95 ± 0.14	$1.37^{+0.23}_{-0.19}$	0.97 ± 0.15	$0.97^{+0.17}_{-0.14}$
EW$_{\rm Fe}$ (eV)	158 ± 23	222^{+37}_{-31}	153 ± 25	152^{+26}_{-22}
$E_{\rm LE}$ (keV)	...	...	$1.968^{+0.050}_{-0.061}$	$1.961^{+0.052}_{-0.072}$
$\sigma_{\rm LE}$ (keV)	...	...	$0.116^{+0.083}_{-0.087}$	$0.124^{+0.093}_{-0.087}$
$I_{\rm LE}$ ($\times 10^{-3}$)	...	...	$1.54^{+0.82}_{-0.54}$	$1.64^{+1.11}_{-0.62}$
EW$_{\rm LE}$ (eV)	...	...	153 ± 25	152^{+25}_{-24}
$E_{{\rm edge}_l}$ (keV)	1.315 ± 0.056	...	...	...
$\tau_{{\rm edge}_l}$	$0.325^{+0.077}_{-0.070}$	...	...	...
$E_{{\rm edge}_h}$ (keV)	...	...	$8.69^{+0.24}_{-0.20}$	$8.69^{+0.24}_{-0.20}$
$\tau_{{\rm edge}_h}$	...	...	0.097 ± 0.029	0.097 ± 0.029
χ^2/dof	245/201	291/204	206/199	206/198

Note.—Uncertainties are at the 90% confidence level for a single parameter. The blackbody normalization ($N_{\rm BB}$) is in units of L_{37}/D_{10}^2, where L_{37} is the luminosity in units of 10^{37} ergs s^{-1} and D_{10} is the distance to the source in units of 10 kpc. The parameters kT_0 and kT_e are the seed photon temperature and the electron temperature, respectively, and τ is the optical depth of the scattering cloud. The Comptt and Compst normalizations, $N_{\rm comp}$, are defined as in XSPEC version 10. The parameter $N_{\rm H,PC}$ indicates the column absorption of the partial covering, and f, the covering fraction. The parameter $f_{\rm bol}$ is the unabsorbed flux in the 0.1–100 keV range of the Comptonized component in units of ergs cm^{-2} s^{-1}. The parameter EW$_{\rm Fe}$ indicates the equivalent width of the line at 6.5 keV, $E_{\rm Fe}$ its centroid and $I_{\rm Fe}$ its intensity in units of photons cm^{-2} s^{-1}, and EW$_{\rm LE}$, $E_{\rm LE}$, and $I_{\rm LE}$ are the same parameters for the low-energy line at 1.9 keV. The parameter $E_{{\rm edge}_l}$ indicates the energy of the absorption edge at low energy, and $\tau_{{\rm edge}_l}$ its relative optical depth. The parameters $E_{{\rm edge}_h}$ and $\tau_{{\rm edge}_h}$ are the same parameters for the edge at high energy.

6%–8% at 2 keV and 5% at 10 keV, much higher than any systematic residuals in the MECS and HPGSPC data with respect to the Crab spectrum.[5] Therefore, we first added an emission line at ~ 1.9 keV, which significantly improved the fit. We obtained a $\chi^2/{\rm dof} = 236/201$, yielding a probability of chance improvement of the fit (with respect to model 2) of $\sim 3.61 \times 10^{-9}$. Then we added an absorption edge at ~ 8.7 keV, obtaining a $\chi^2/{\rm dof} = 206/199$ and a probability of chance improvement of the fit (with respect to the previous model) of $\sim 3.51 \times 10^{-5}$. These two features fall at the ends of the MECS energy range. We note that no problems are known to exist in the MECS response matrix at the ends of the energy range, and the MECS spectra of many sources as bright as X1822−371 (or even brighter) have been published without any need for features at 2 or 8 keV. However, we wanted to be sure that such features could not be a result of instrumental systematics. Using a reduced energy range for the MECS (3–8 keV), these features are still statistically significant, giving probabilities of chance improvement of the fit of $\sim 5 \times 10^{-3}$ and $\sim 1.8 \times 10^{-5}$ for the low-energy line and the absorption edge, respectively. We also tried to fit the *BeppoSAX* spectrum using the whole MECS range (1.8–10 keV) and ignoring all the HPGSPC points below 10 keV. Again the addition of the edge at 8.5 keV was statistically significant ($\sim 10^{-5}$), demonstrating that this feature is present in both the MECS and the HPGSPC data. We therefore conclude that these features, which are also expected to be emitted in photoionized ADCs (see, e.g., Ko & Kallman 1994; Kallman et al. 1996), are most probably real and not instrumental effects.

The values of the parameters corresponding to the best-fit model are reported in Table 1 (model 3). We plot in Figure 2 (*bottom*) the residuals in units of σ with respect to model 3, and in Figure 3 the unfolded spectrum corresponding to this model.

In order to obtain some information about the seed photon temperature of the Comptonization spectrum, we tried the Comptt model (Titarchuk 1994) instead of the Compst model. We obtain an equivalently good fit (see Table 1, model 4). However, because the seed photon temperature is close to the low-energy end of our spectral range, we can only estimate an upper limit to this temperature of ~ 0.2 keV.

To summarize, a brief description of the best-fit parameters follows: We obtained a hydrogen equivalent column $N_{\rm H} \simeq 1.2 \times 10^{21}$ cm^{-2}. The hydrogen equivalent column of the partial covering is $N_{\rm H,PC} \simeq 4.5 \times 10^{22}$ cm^{-2}, and the covered region corresponds to a fraction of 71% of the total. The Comptonized component has an electron temperature of $kT_e \sim 4.7$ keV and optical depth $\tau \sim 14$ for a spherical geometry. We find a broad emission line at ~ 6.5 keV with FWHM $= 0.70$ keV and equivalent width of ~ 150 eV. An emission line at ~ 1.9 keV with FWHM $= 0.27$ keV and equivalent width of ~ 54 eV and

[5] See footnote 4.

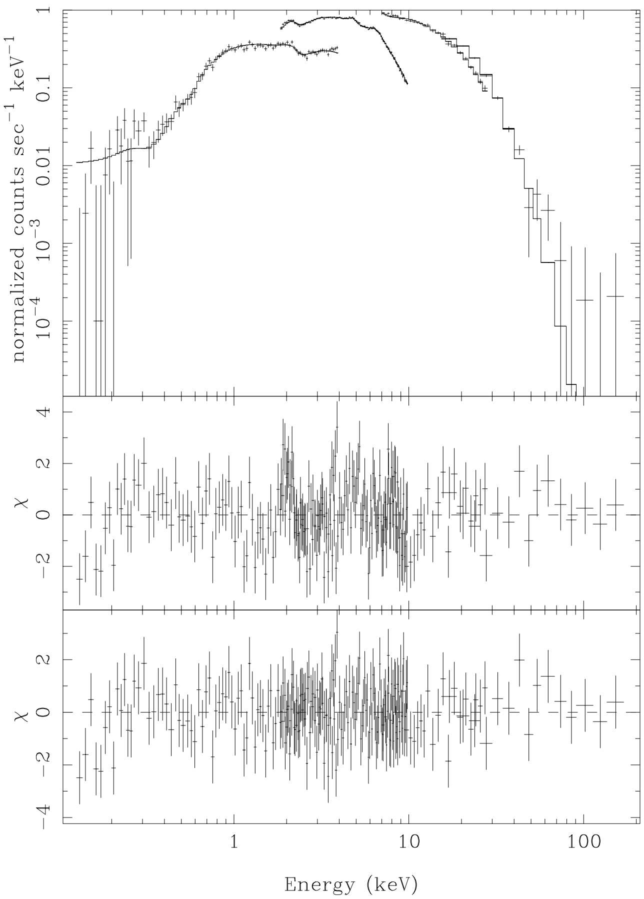

FIG. 2.—Energy spectra (0.1–200 keV) of X1822−371. *Top*, data and model 2 (see Table 1); *middle*, residuals in units of σ with respect to model 2; *bottom*, residuals in units of σ with respect to the best-fit model (model 3).

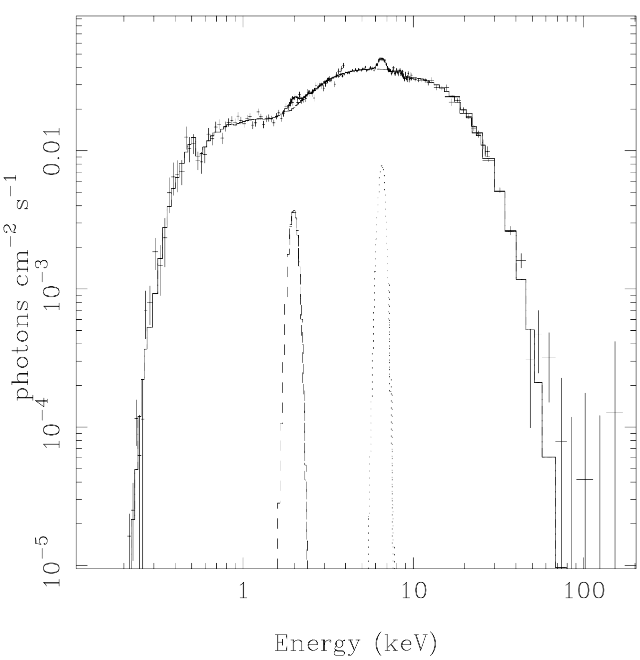

FIG. 3.—Unfolded spectrum of X1822−371 and the best-fit model (model 3). The single components of the model are also shown. The solid line is the Compst model with partial covering. The low-energy line at ∼1.9 keV (*dashed line*) and the iron emission line at ∼6.5 keV (*dotted line*) are also shown. The absorption edge at 8.7 keV is visible.

an absorption edge at ∼8.7 keV with optical depth $\tau_{\rm max} \sim 0.1$ are also detected with high statistical significance.

3. DISCUSSION

We have analyzed data from a 43 ks *BeppoSAX* observation for the dipping source X1822−371 in the energy range 0.1–200 keV. We obtained the best fit to these data using a partially covered Comptonization model, plus two emission lines and an absorption edge. The results of our spectral analysis of X1822−371 are discussed in the following.

We obtained an equivalent absorption column of $N_{\rm H} \sim 1.2 \times 10^{21}$ cm^{-2}. For a distance to the source of 2.5 kpc (Mason & Cordova 1982), the visual extinction in the direction of X1822−371 is $A_v = 0.87 \pm 0.32$ mag (Hakkila et al. 1997). Using the observed correlation between visual extinction and absorption column (Predehl & Schmitt 1995), we find $N_H = (1.02 \pm 0.02) \times 10^{21}$ cm^{-2}. This value is much higher than the value obtained by Parmar et al. (2000) and by using our model 1. On the other hand, the expected Galactic absorption is in perfect agreement with the value that we obtained using models 3 and 4. In our model, the Comptonization spectrum is partially absorbed because of the presence of excess matter close to the source, obscuring part of the emission region. The absorption column of this partial covering is ∼4.5×10^{22} cm^{-2}, an order of magnitude larger than the Galactic absorption, and covers a fraction of ∼71% of the source spectrum.

The continuum is well fitted by a Comptonization spectrum, probably produced in a hot ($kT_e \sim 4.7$ keV) region of moderate optical depth ($\tau \sim 14$ for a spherical geometry) surrounding the neutron star. Note that in this spectral deconvolution there is no need for a soft blackbody. This component is needed to fit the soft emission of the source when the partial covering is not used, as in model 1 of Table 1, i.e., the model adopted by Parmar et al. (2000). In this case, the measured contribution of the blackbody to the 1–10 keV flux is greater than 40%. In this scenario, as already noted by Parmar et al. (2000), the blackbody component is most probably emitted in the inner part of the system (i.e., from an optically thick boundary layer close to the neutron star's surface or from the neutron star itself). It is therefore unlikely to be observed directly in a high-inclination (∼85°) source such as X1822−371. One can suppose that part of the blackbody emission can be scattered into the line of sight by the corona. However, because the optical depth of this corona, as deduced by fitting its spectrum with Comptonization models, is $\tau \gtrsim 10$ (see Table 1 and Parmar et al. 2000), any blackbody spectrum passing through it will be (almost) completely reprocessed. Then the blackbody should contribute a low percentage of the total source luminosity or should not be present. We believe that a more reasonable scenario is the one proposed by our models 3 and 4, in agreement with the optically thick scenario used by Heinz & Nowak (2001) to fit simultaneous *RXTE* and *ASCA* observations.

The Comptonized component probably originates in an ADC that could be formed by evaporation of the outer layers of the disk illuminated by the emission of the central object (White & Holt 1982). The radius of the corona can be written as $R_c \simeq [M_{\rm NS}/(1\ M_\odot)]T_7^{-1}\ R_\odot$ (White & Holt 1982), where $M_{\rm NS}$ is the mass of the compact object, $M_\odot$ and $R_\odot$ are mass and radius of the Sun, and T_7 is the ADC temperature in units of 10^7 K. Under this hypothesis, using the values reported in Table 1 (model 3), we find that the radius of the ADC is $R_c \simeq 1.8 \times 10^5$ km. Similar values for the ADC radius are reported by White & Holt (1982; $R_c \simeq 2 \times 10^5$ km) and by Heinz & Nowak (2001; $R_c \simeq 2.9 \times 10^5$ km) for X1822−371. Using the relation $\tau = \sigma_T N_e R_c$, we can infer the density of the ADC, where τ is the optical depth obtained by the fit, σ_T is the Thomson cross section, N_e is the number of particles per unit volume and R_c is the ADC radius calculated above. Note that we are considering N_e constant along the radius of the corona, which is a rough approximation. Under this hypothesis we find $N_e \simeq 1.15 \times 10^{15}$ cm^{-3}. This value is in line with previous simulations of the ADC (Vrtilek, Soker, & Raymond 1993). In fact, considering an inclination angle of 85° (i.e., an angle of $\sim 5°$ from the disk plane), Vrtilek et al. (1993, their Fig. 2) find a density along the line of sight in the ADC corona of around 10^{15} cm^{-3}. Following Frank, King, & Lasota (1987) and using the orbital parameters reported by Parmar et al. (2000), we estimate that the accretion disk radius is $R_d \sim 4.3 \times 10^5$ km, similar to the value $R_d \simeq 4 \times 10^5$ km obtained by White & Holt (1982). The disk radius is therefore larger than the estimated radius of the ADC, as expected. In particular, the ratio between the accretion disk radius and the coronal radius is $R_d \simeq 2.4 R_c$.

Our proposed model is also in agreement with the general behavior of high-inclination dipping sources (see, e.g., Balucinska-Church et al. 2000; Smale et al. 2000 and references therein). The model used to describe their spectra consists of a pointlike blackbody emission and a Comptonized component from the ADC. The spectral evolution during the dips, when we observe the source emission through the thickened region of the accretion disk rim, can be described in terms of a "progressive covering" given by an absorber moving progressively across the emission regions. While the blackbody is rapidly absorbed, suggesting that it is emitted by a compact region (probably from the neutron star), the Comptonized component is partially absorbed, suggesting that its emission region (i.e., the ADC) is extended. In particular, in the case of X1624−490, Smale et al. (2000) showed that the ADC has a larger angular size than the absorber and has a height-to-radius ratio of $\sim 10\%$ with an estimated coronal radius of $\sim 5 \times 10^5$ km (similar to the value we found above for X1822−371). The spectrum of X1822−371 is very similar to these dip spectra, with its lack of the blackbody component (which is probably completely absorbed) and partially covered Comptonized component. Therefore, in this case of very high inclination, we probably always observe the source emission through the thickened accretion disk. The presence of a thickened outer disk is also suggested by the recent *XMM-Newton* results on EXO 0748−67 (Cottam et al. 2001). The presence of a wealth of emission lines and absorption edges in the range between 0.4 and 1 keV, showing no eclipses or other modulations related to the orbital phase and large widths probably due to velocity broadening, suggests that these low-energy features are emitted in a flared accretion disk extending high above the equatorial plane (Cottam et al. 2001).

From the spectral fitting of X1822−371, we obtained that a fraction of 71% of the Comptonization spectrum is absorbed by an excess of matter. We suppose that this matter is close to the equatorial plane, at the outer rim of the disk. Considering the area of the ADC, $A_{\rm ADC} = 4\pi R_c^2$, and the area of the covered region as $A_{\rm cov} = 4\pi R_c h$, where h is the height of the absorbing matter above the disk, we can write

$$\frac{A_{\rm cov}}{A_{\rm ADC}} = \frac{h}{R_c} \simeq 0.71 \ . \tag{1}$$

From this equation we find that the angle subtended by the absorbing region is $\theta \sim 16°$, adopting the disk radius reported above. This scenario is in agreement with the lack of any soft component in our spectral deconvolution. In fact, the inner region could be either reprocessed by the optically thick ADC or absorbed by the excess matter at the outer accretion disk originating the partial covering.

Having the temperature of the seed photons for the Comptonization, we can derive the radius of the seed photon–emitting region. Following in't Zand et al. (1999), this radius can be expressed as $R_W = 3 \times 10^4 D[f_{\rm bol}/(1+y)]^{1/2}/(kT_0)^2$ km, where D is the distance of the source in kiloparsecs, $f_{\rm bol}$ is the unabsorbed flux in ergs cm^{-2} s^{-1}, kT_0 is the seed photon temperature in keV, and $y = 4kT_e \tau^2/m_e c^2$ is the relative energy gain due to the Comptonization. We obtain from the fit an upper limit for the seed photon temperature (see Table 1, model 4). Using this upper limit in the formula above, we obtain a lower limit for the seed photon radius of ~ 24 km. We can suppose that these photons come from the inner region of the system, as the neutron star or the boundary layer between the neutron star and the accretion disk, the inner radius of the accretion disk, or both these regions.

Another component of the model is an emission line at 6.5 keV with an equivalent width of ~ 150 eV. This is probably a result of fluorescence of moderately ionized iron. A possible origin of the emission line could be Compton reflection of the photons from the ADC by the accretion disk (George & Fabian 1991; Matt, Perola, & Piro 1991). However, the large value of the equivalent width seems to be incompatible with this interpretation. In fact, for inclinations larger than 80°, the iron-line equivalent width should have a value of ~ 20 eV (Brandt & Matt 1994). Moreover, the iron-line equivalent width has a maximum value of ~ 130 eV for an isotropic source covering half of the sky ($\Omega/2\pi = 1$), as seen by the reflector, and with an inclination angle of the system of $i = 0°$. On the other hand, there are indications suggesting that the emission line in X1822−371 originates in the ADC. In fact, according to Vrtilek et al. (1993), when the iron emission line originates in the ADC, its equivalent width increases with increasing inclination angle: for $i \sim 80°$, the equivalent width is ~ 150 eV (see Vrtilek et al. 1993, their Fig. 6). This is in agreement with our results for X1822−371, for which we obtain an equivalent width of the emission iron line of ~ 150 eV for $i \sim 85°$ (the inclination angle of X1822−371). Note that the ADC origin (instead of the disk origin) of the iron line is also in agreement with our spectral modeling of the continuum, in which the emission from the accretion disk is not directly observed.

The iron line we observe in X1822−371 is quite broad (~ 0.7 FWHM). Since we have excluded a disk origin for this line, we cannot explain its broadening with the standard scenario adopted for active galactic nuclei (AGNs) containing massive black holes, where the broadening of the iron line is thought to be the result of general relativistic effects in the innermost regions of an accretion disk. In the case of coronal origin of the iron line, its width can be explained by Compton scattering of the line photons in the optically thick plasma surrounding the central X-ray source. This produces a genuinely broad Gaussian distribution of line photons, with $\sigma \gtrsim E_{\mathrm{Fe}}(kT_e/m_e c^2)^{1/2}$, where E_{Fe} is the centroid energy of the iron line and kT_e is the electron temperature in the ADC. More detailed calculations, in which the dependence on the optical depth is taken into account, show that this effect can explain the width of the iron line for temperatures of the emitting region of a few keV (Kallman & White 1989; see also Brandt & Matt 1994). The presence of several unresolved components from many iron ionization stages (line blending) can also contribute to the line broadening. In this case the single components could be resolved by the new high-resolution instruments on board *Chandra* and *XMM-Newton*. The observation of a broad iron line whose width cannot be explained by relativistic Doppler effects in the innermost region of an accretion disc is interesting and suggests alternative explanations, the most probable of which is Comptonization, for the line broadening in LMXBs. However, it is important to observe that Comptonization fails to explain the shape of the line in AGNs, for which the most probable broadening mechanism is relativistic Doppler effects (e.g., Ruszkowski et al. 2000; Misra 2001).

We observe another emission line at ~ 1.9 keV with an equivalent width of ~ 54 eV. This line could be a result of emission from the L shell of ionized iron (Fe XXIII–Fe XXIV for plasma densities of $\sim 10^{11}$ cm^{-3}; see Kallman et al. 1996) or from the K shell of highly ionized Si or Mg. The emission region of this line could be the outer region of the ADC at high latitude ($>15°$), where the coronal density is expected to be around 10^{11}–10^{12} cm^{-3} (Vrtilek et al. 1993). The last component is an absorption edge at ~ 8.7 keV with an optical depth of ~ 0.1. Following Turner et al. (1992) for a correspondence between iron edge energy and ionization level, this edge corresponds to Fe XXIV. This suggests the presence of highly ionized material around the compact object. The best-fit value for the optical depth τ_{edge}, considering the photoionization cross section for the K shell of Fe XXIV (Krolik & Kallman 1987), corresponds to a hydrogen column density of $\sim 1.3 \times 10^{23}$ cm^{-2}, assuming cosmic abundance of iron. This is 2 orders of magnitude higher than the measured Galactic absorption and 1 order of magnitude higher than the neutral matter responsible for the partial covering (see Table 1, models 3 and 4). From the estimation of the coronal density N_e reported above, we can derive the corresponding hydrogen column density in the ADC, which is roughly 2×10^{25} cm^{-2}. This suggests that a part of the ADC could be (photo-) ionized and responsible for the presence of both the iron edge and the low-energy emission line.

4. CONCLUSIONS

We analyzed data from a *BeppoSAX* observation of X1822−371 performed in 1997 September 9 and 10. The energy spectrum is well described by a Comptonized spectrum with partial covering, two iron emission lines, and an absorption edge. The Comptonized spectrum is probably produced in the ADC, with electron temperature of ~ 4.7 keV and with moderate optical depth ($\tau \sim 14$ for a spherical geometry). The partial covering could be due to excess neutral matter placed close to the equatorial plane at the outer rim of the accretion disk, forming a thickened outer disk subtending an angle of $\sim 16°$ as seen from the neutron star. The high inclination of the source ($\sim 85°$) and the presence of the cloud of neutral matter above the accretion disk does not allow us to observe the direct emission from the neutron star and the inner accretion disk. In the spectrum, an iron emission line is present at ~ 6.5 keV with a large equivalent width of 150 eV. We showed that this line cannot come from the accretion disk but is probably produced in the ADC. Another emission line at ~ 1.9 keV with an equivalent width of 54 eV and an absorption edge at ~ 8.7 keV are also detected in the spectrum, which could be produced in an ionized region in the ADC.

This work was supported by the Italian Space Agency via the Ministero dell' Università della Ricerca Scientifica e Tecnologica.

REFERENCES

Balucinska-Church, M., Humphrey, P. J., Church, M. J., & Parmar, A. N. 2000, A&A, 360, 583
Boella, G., Butler, R. C., Perola, G. C., Piro, L., Scarsi, L., & Blecker, J. 1997, A&AS, 122, 299
Brandt, W. N., & Matt, G. 1994, MNRAS, 268, 1051
Cottam, J., Kahn, S. M., Brinkman, A. C., den Herder, J. W., & Erd, C. 2001, A&A, 365, L277
Frank, J., King, A. R., & Lasota, J.-P. 1987, A&A, 178, 137
George, I. M., & Fabian, A. C. 1991, MNRAS, 249, 352
Hakkila, J., Myers, J. M., Stidham, B. J., & Hartmann, D. H. 1997, AJ, 114, 2043
Heinz, S., & Nowak, M. A. 2001, MNRAS, 320, 249
Hellier, C., & Mason, K. O. 1989, MNRAS, 239, 715
Hellier, C., Mason, K. O., & Williams, O. R. 1992, MNRAS, 258, 457
in't Zand, J. J. M., et al. 1999, A&A, 345, 100
Kallman, T. R., Liedahl, D., Osterheld, A., & Goldstein, W. 1996, ApJ, 465, 994
Kallman, T., & White, N. E. 1989, ApJ, 341, 955
Ko, Y., & Kallman, T. 1994, ApJ, 431, 273
Krolik, J. H., & Kallman, T. R. 1987, ApJ, 320, L5
Mason, K. O., & Cordova, F. A. 1982, ApJ, 262, 253
Matt, G., Perola, G. C., & Piro, L. 1991, A&A, 247, 25
Misra, R. 2001, MNRAS, 320, 445
Parmar, A. N., Oosterbroek, T., Del Sordo, S., Segreto, A., Santangelo, A., Dal Fiume, D., & Orlandini, M. 2000, A&A, 356, 175
Predehl, P., & Schmitt, J. H. M. M. 1995, A&A, 293, 889
Ruszkowski, M., Fabian, A. C., Ross, R. R., & Iwasawa, K. 2000, MNRAS, 317, L11
Smale, A. P., Church, M. J., & Balucinska-Church, M. 2001, ApJ, 550, 962
Sunyaev, R. A., & Titarchuk, L. 1980, A&A, 86, 121
Titarchuk, L. 1994, ApJ, 434, 570
Turner, T. J., Done, C., Mushotzky, R., & Madejski, G. 1992, ApJ, 391, 102
Vrtilek, S. D., Soker, N., & Raymond, J. C. 1993, ApJ, 404, 696
White, N. E., & Holt, S. S. 1982, ApJ, 257, 318